doi:10.1093/brain/awu398 BRAIN 2015: 138; 736–745 | 736

BRAIN
A JOURNAL OF NEUROLOGY

Molecular disorganization of axons adjacent to human lacunar infarcts

Jason D. Hinman,[1] Monica D. Lee,[1] Spencer Tung,[2] Harry V. Vinters[1,2] and S. Thomas Carmichael[1]

Cerebral microvascular disease predominantly affects brain white matter and deep grey matter, resulting in ischaemic damage that ranges from lacunar infarcts to white matter hyperintensities seen on magnetic resonance imaging. These lesions are common and result in both clinical stroke syndromes and accumulate over time, resulting in cognitive deficits and dementia. Magnetic resonance imaging studies suggest that these lesions progress over time, accumulate adjacent to prior lesions and have a penumbral region susceptible to further injury. The pathological correlates of this adjacent injury in surviving myelinated axons have not been previously defined. In this study, we sought to determine the molecular organization of axons in tissue adjacent to lacunar infarcts and in the regions surrounding microinfarcts, by determining critical elements in axonal function: the morphology and length of node of Ranvier segments and adjacent paranodal segments. We examined post-mortem brain tissue from six patients with lacunar infarcts and tissue from two patients with autosomal dominant retinal vasculopathy and cerebral leukoencephalopathy (previously known as hereditary endotheliopathy with retinopathy, nephropathy and stroke) who accumulate progressive white matter ischaemic lesions in the form of lacunar and microinfarcts. In axons adjacent to lacunar infarcts yet extending up to 150% of the infarct diameter away, both nodal and paranodal length increase by ~20% and 80%, respectively, reflecting a loss of normal cell-cell adhesion and signalling between axons and oligodendrocytes. Using premorbid magnetic resonance images, brain regions from patients with retinal vasculopathy and cerebral leukoencephalopathy that harboured periventricular white matter hyperintensities were selected and the molecular organization of axons was determined within these regions. As in regions adjacent to lacunar infarcts, nodal and paranodal length in white matter of these patients is increased. Myelin basic protein and neurofilament immunolabelling demonstrates that axons in these adjacent regions have preserved axonal cytoskeleton organization and are generally myelinated. This indicates that the loss of normal axonal microdomain architecture results from disrupted axoglial signalling in white matter adjacent to lacunar and microinfarcts. The loss of the normal molecular organization of nodes and paranodes is associated with axonal degeneration and may lead to impaired conduction velocity across surviving axons after stroke. These findings demonstrate that the degree of white matter injury associated with cerebral microvascular disease extends well beyond what can be identified using imaging techniques and that an improved understanding of the neurobiology in these regions can drive new therapeutic strategies for this disease entity.

1 Departments of Neurology, David Geffen School of Medicine, University of California Los Angeles, USA
2 Department of Pathology and Laboratory Medicine, Section of Neuropathology, David Geffen School of Medicine, University of California Los Angeles, USA

Correspondence to: Jason D. Hinman, M.D., Ph.D.,
University of California Los Angeles,
Department of Neurology,
Neuroscience Research Building,
635 Charles E. Young Dr. South, Room 415
Los Angeles, CA 90095, USA
E-mail: jhinman@mednet.ucla.edu

Received May 30, 2014. Revised November 3, 2014. Accepted November 19, 2014. Advance Access publication January 22, 2015
© The Author (2015). Published by Oxford University Press on behalf of the Guarantors of Brain. All rights reserved.
For Permissions, please email: journals.permissions@oup.com

Keywords: lacunar stroke; small vessel disease; neuropathology; vascular dementia; ion channels

Abbreviations: DTI = diffusion tensor imaging; RVCL = retinal vasculopathy and cerebral leukoencephalopathy

Introduction

Microvascular ischaemic disease of the brain predominantly affects the poorly collateralized deep white matter and deep grey matter. Infarcts affecting subcortical structures account for up to 25% of clinical stroke presentations (Roger *et al.*, 2012) and the prevalence of subclinical ischaemic damage to white matter is estimated between 6% and 25% (Go *et al.*, 2014) and increases with age (Vermeer *et al.*, 2007). These silent subclinical events contribute significantly to the risk of large vessel stroke (Vermeer *et al.*, 2003; Arsava *et al.*, 2011), disability (Sonohara *et al.*, 2008), vascular dementia (DeCarli, 2013) and death (Conijn *et al.*, 2011). Despite the severity and frequency of these lesions, data on how they affect the molecular and cellular elements of brain white matter remain limited.

The neuroimaging appearance of such lesions varies dramatically from frank lacunar infarcts to white matter hyperintensities on T_2/FLAIR sequences. Fisher classically defined lacunar infarcts as <15 mm^3 in maximal dimension (Fisher, 1982) and occurring deep within the brain. With the introduction of ultra-high field MRI scanning, *in vivo* demonstration of microinfarcts, generally $<500\,\mu$m in size (Brundel *et al.*, 2012), indicates that subclinical microvascular injury may be much more common than previously thought (van Veluw *et al.*, 2013) and plays a significant role in the development of dementia and cognitive impairment (Okamoto *et al.*, 2009). Serial imaging studies indicate that new lacunes develop adjacent to previous ones (Duering *et al.*, 2013) whereas diffusion tensor imaging (DTI) suggest that there is a penumbra of injury that exists adjacent to well-defined lacunar lesions, reflecting more subtle tissue damage (Maillard *et al.*, 2011) with an increased susceptibility to additional injury. Recent data suggests that DTI may not correlate well with the axonal pathology seen in brain white matter in patients with multiple sclerosis (Zollinger *et al.*, 2011), therefore we sought to determine the molecular organization of axons in tissue adjacent to lacunar infarcts and in regions surrounding microinfarcts. Prior human pathological studies have not applied our enhanced understanding of the biology of myelinated axons to better characterize the full extent of white matter injury after stroke (Bailey *et al.*, 2012).

Myelinated axons develop regional specializations that result in clustering of molecules needed for saltatory conduction, including voltage-gated sodium channels (Na_V) at the node of Ranvier (Susuki and Rasband, 2008). Adjacent regions, termed paranodes, cluster molecules that mediate cell-cell adhesion and trophic signalling between the axon and the oligodendrocyte (Einheber *et al.*, 1997; Rios *et al.*, 2000; Tait *et al.*, 2000; Bhat *et al.*, 2001; Boyle *et al.*, 2001; Schafer and Rasband, 2006). Disruption of axonal microdomains has been well studied in multiple sclerosis. In multiple sclerosis, autoimmune destruction of the myelin sheath disrupts axoglial contact and leads to elongated paranodes and a redistribution of Na_V along the length of the axon (Dupree *et al.*, 1999; Reimer *et al.*, 2011). Over time, this redistribution of Na_V outside of the normal nodal region causes axonal damage contributing to disease progression (Wingerchuk *et al.*, 2001). Thus, precise formation and maintenance of axonal microdomains is a *de facto* measurement of white matter health and their loss indicates disrupted axoglial signalling and predisposes to axonal degeneration.

Here, we examined human post-mortem tissue adjacent to defined lacunar and microinfarct lesions for the molecular organization of surviving axons. We determined axonal microdomain integrity at the nodal and paranodal regions within these surviving axons. We identified abnormal appearing nodal and paranodal segments extending significant distances from the central core of the lacunar infarct, supporting imaging observations that the full extent of white matter injury extends substantially beyond that observed using macroscopic techniques. We also examined axonal microdomain integrity in the white matter of two rare cases of autosomal dominant retinal vasculopathy and cerebral leukoencephalopathy (RVCL) harbouring multiple microinfarcts corresponding to T_2/FLAIR hyperintensities on MRI.

Materials and methods

Clinical case selection

The cases selected for examination in this study are a retrospective, convenience sample of autopsy cases from a clinicopathological study of cognitively normal subjects, those with subcortical ischaemic vascular dementia or Alzheimer's disease. Written informed consent for autopsy was obtained from all subjects or legal next-of-kin. From this larger database, cases selected for detailed microscopy included those with definable small vessel infarcts determined by expert neuropathological assessment of haematoxylin and eosin stained sections. Demographic information and anatomical location of infarcts for each case are detailed in Table 1. Based on the clinical information available at autopsy, all the lesions identified were presumed to be asymptomatic in life. In addition, post-mortem tissue examination of two subjects with a genetically confirmed diagnosis of autosomal dominant RVCL [formerly hereditary endotheliopathy with retinopathy, nephropathy and stroke (HERNS)] syndrome, were also included in the study (Jen *et al.*, 1997; Kolar *et al.*, 2014).

Table 1 Clinical demographics

Case ID	Age (years)	Sex	Infarct location	Post-mortem interval (h)	Medical co-morbidities
1	89	F	Right and left basal ganglia	<2	Alzheimer's disease
2	91	F	Basal ganglia	5	Hypertension, coronary artery disease, dementia
3	77	M	Basal ganglia	34	Fronto-temporal dementia
4	85	F	Pons	Unknown	Coronary artery disease, asthma, dementia
5	96	F	Right and left basal ganglia	Unknown	Alzheimer's disease
6	86	M	Caudate	93	Stroke, coronary artery disease, peripheral vascular disease, chronic obstructive pulmonary disease
RVCL #1	52	M	Multiple	24	RVCL, coronary artery disease
RVCL #2	58	F	Multiple	Unknown	RVCL

Tissue processing and immunohistochemistry

Autopsy and brain extractions were performed according to standard procedures. Post-mortem intervals are detailed in Table 1. Extracted brains were immediately fixed in 10% formalin for 2 weeks. Fixed specimens were then blocked for regions of interest, processed and embedded in paraffin. Six-micrometre thick tissue sections were generated from the paraffin embedded blocks for histological analysis using immunofluorescent labelling as follows. Sections were first baked at 60°C melt the paraffin wax and subsequently washed in xylene to dissolve residual paraffin followed by graded ethanol baths (100–70%) and double-distilled H_2O to rehydrate the tissue. For histological staining, sections were then immersed in Harris haematoxylin (Fisher) for 1 min and slightly destained in 1% HCl in 80% ethanol. Haematoxylin-stained slides were further developed with 0.2% ammonia water and then immersed in eosin-Y (Fisher) for 3 min. Following eosin immersion, sections were dehydrated in graded ethanol baths (70–100%), cleared in xylenes and cover-slipped for visualization by light microscopy.

All of the sporadic cases of lacunar infarcts were immunostained for amyloid-$\beta_{1–40}$ (EMD Millipore) and amyloid-$\beta_{1–42}$ (EMD Millipore) as well as tau (Pierce) as part of the routine autopsy assessment. Tissue blocks stained included frontal, superior temporal, occipital, hippocampus, basal ganglia and cerebellum.

For immunofluorescent labelling, tissue epitopes were exposed with heat-induced antigen retrieval using a pressurized antigen decloaking chamber at 120°C for 5 min in 10 mmol citrate pH 6.0 and allowed to cool to room temperature. After antigen retrieval, tissue sections were permeabilized with 0.3% Triton™ X-100 in phosphate-buffered saline (PBS) followed by 5% acetic acid in 95% ethanol. After permeabilization, sections were blocked with 5% normal donkey serum 0.3% Triton™ X-100 in PBS (NDSX) for 1 h. Finally, sections were incubated overnight sequentially with the following primary antibodies: rabbit anti-beta-IV spectrin (1:400; gift from Dr Matthew Rasband, Baylor College of Medicine), mouse anti-contactin-associated protein (caspr) (1:500, Neuromab) (caspr is now known as CNTNAP1), mouse anti-human myelin basic protein (MBP) (1:1000, Chemicon), or rabbit anti-neurofilament 200 (NF200) (1:500, Sigma) in NDSX, visualized using appropriate immunoflourescent anti-mouse (Invitrogen A21202) and anti-rabbit secondary (Invitrogen A10042) antibodies diluted at 1:200 in NDSX and mounted in medium containing DAPI for nuclear counterstaining (Invitrogen P36935).

Imaging and quantification

Histological sections stained for haematoxylin and eosin were imaged on a Leica DMLB microscope. Lacunar infarcts were identified by the loss of tissue associated with cavitary lesions. When no cavitary lesion was present, the lesion was identified by the loss of histological staining and associated tissue pallor. Infarct areas were measured using Stereo Investigator® (MBF Inc.) (Supplementary Table 1). Although most infarcts were elliptically shaped, areas were measured by tight perimeter enclosures using the contour feature in Stereo Investigator®. A centre point of each lesion was identified and the horizontal and vertical diameters measured. Immunolabelled serial sections were imaged at ×60–100 using a Nikon C2 laser scanning confocal microscope. The region containing the infarct was defined and high-powered microscopic fields were imaged at distances corresponding to 50% tertiles of the infarct diameter away from the centre of the infarct in both vertical and horizontal directions, while remaining within the surrounding white matter. Five microscopic fields were imaged per tertile. For nodal and paranodal measurements, only axons with an identifiable node and two adjacent paranodes were measured to avoid measuring axonal microdomains that were cut during thin sectioning. The number of infarcts and total nodal and paranodal measurements are listed in parentheses in Table 2. Control nodal and paranodal measurements were determined using both an internal control (obtained by measuring segments from regions of white matter far away from the region of lacunar infarct) and external controls from age-matched samples without evidence of infarct. Statistical significance of changes in nodal and paranodal length were determined using a one-tailed Student's *t*-test assuming unequal variance and $P < 0.05$.

Results

Molecular organization of axons in human lacunar infarcts

To determine the molecular organization of axons adjacent to lacunes, we selected six clinical cases with

Table 2 Nodal and paranodal length in axons adjacent to human lacunar infarcts

	Nodal length (μm)	*P*-value	% Change	Paranodal length (μm)	*P*-value	% Change
External control (*n* = 2/600)	0.88	n/a	n/a	2.16	n/a	n/a
Internal control (n = 2/178)	0.83	n/a	n/a	2.03	n/a	n/a
WMS 10–50% (*n* = 8/162)	1.05	0.00322	19.66	3.96	5.38758×10^{-31}	83.20
WMS 50–100% (*n* = 8/338)	1.09	3.15726×10^{-7}	25.11	4.21	1.72034×10^{-63}	95.02
WMS 100–150% (*n* = 8/350)	1.04	5.18205×10^{-6}	19.33	4.12	4.8797×10^{-61}	90.79

n/a = not applicable; WMS = white matter stroke.

eight different lacunes. The age, sex, infarct location, post-mortem interval, and medical co-morbidities of each case are presented in Table 1. The patients selected ranged in age from 77 to 96 years. Nearly all of the subjects carried a pre-mortem diagnosis of dementia. This compares to other studies of white matter ischaemic pathology series in which 50% of cases had a clinical diagnosis of dementia and 100% of cases had Alzheimer's disease or ischaemic vascular dementia (Fernando *et al*., 2004). Although several of the cases had a pathological diagnosis of Alzheimer's disease (Supplementary Table 1), no significant immunolabelling for amyloid-$\beta_{1\text{-}40}$ or amyloid-$\beta_{1\text{-}42}$ was detectable in the tissue blocks containing the lacunar infarcts (Supplementary Fig. 1).

Lacunar infarcts were defined pathologically by the presence of a focal necrotic cystic cavity by haematoxylin-eosin staining, conforming to a classic type I cavitary lacunar lesion, or regions of a definable area of tissue pallor; i.e. type Ib lesion (Ferrer *et al*., 2008). The diameter (in μm) and area (in mm^2) of each defined region of lacunar stroke was measured and is presented in Supplementary Table 1. Most of the infarcts were substantially smaller than Fisher's classical definition of an infarct measuring <15 mm^3 and were predominantly localized within white matter. Representative haematoxylin and eosin stained sections of a classical lacune within subcortical white matter and a more subtle infarct without a central necrotic core of tissue loss are shown in Supplementary Fig. 2. Immunolabelling of control white matter for beta-IV spectrin to label nodes of Ranvier and contactin-associated protein (caspr) to label paranodes reveals a staining pattern with relatively uniform nodal and paranodal length within compact white matter (Supplementary Fig. 3). Immunolabelling of nodes and paranodes in normal-appearing white matter several centimetres from the defined infarct shows a similarly uniform organization of beta-IV spectrin and caspr within nodes and paranodes, respectively (Fig. 1A). Adjacent to lacunar stroke, paranodal staining with caspr reveals a relative loss of caspr-positive paranodal profiles when compared to the uniform staining seen in external and internal control sections (Fig. 1B). When present adjacent to infarcts, caspr-positive paranodal segments were elongated (inset, Fig. 1B). Beta-IV spectrin-positive nodal segments demonstrated relative preservation of nodal density when compared to external and internal controls, but also demonstrated morphologic disruption including elongation of nodal segments (Fig. 1B).

We hypothesized that the molecular organization of axons would become more normal appearing with a greater distance from the infarct core as the degree of ischaemia, inflammatory response and gliosis associated with lacunar infarcts diminishes. As the infarcts included in this study varied greatly in diameter, we established a method for quantification of axonal abnormalities based on the individual infarct diameter. Molecular disruption of axons was then measured in adjacent white matter as a percentage of the individually measured infarct diameter, divided into tertiles extending up to 150% of the infarct diameter away from the central core (Supplementary Fig. 4).

Regions of white matter immediately adjacent to the infarct (10–50% of the infarct diameter) demonstrated multiple irregularities in the appearance of nodal and paranodal segments (Fig. 2A). Morphologic disruption of nodal segments was frequently seen in this region and quantification of nodal length in this region reveals a ~20% increase compared to external controls ($P = 0.003$, Table 2). In this region immediately adjacent to the infarct cavity, paranodal segments were similarly disrupted with an 83.2% increase in average paranodal length when compared to control ($P < 0.0001$, Table 2). As distance from the infarct core increases to 50–100% of the infarct diameter away, nodal and paranodal abnormalities persist (Fig. 2B), with a significant increase in nodal and paranodal segment length compared to control (25.1% and 95.0%, respectively, Table 2). In the furthest regions from the infarct centre, 100–150% of the infarct diameter or over twice the diameter of the infarct centre, molecular disruption of axons persists with morphologic disruption of nodal and paranodal segments (Fig. 2C), as well as a similar significant 19.3% increase in nodal length and a 90.8% increase in paranodal length (Table 2). Similar nodal and paranodal length measurements were obtained from both internal controls (same section, at least 1 cm away from infarct) and external controls (Table 2). Figure 3A highlights beta-IV spectrin immunoreactivity at the axon initial segment, which was excluded from quantification in this study. These results indicate that the molecular disruption of axons adjacent to white matter infarcts can extend between 187 to 2106 μm from the infarct core, depending on its size (Supplementary Table 1).

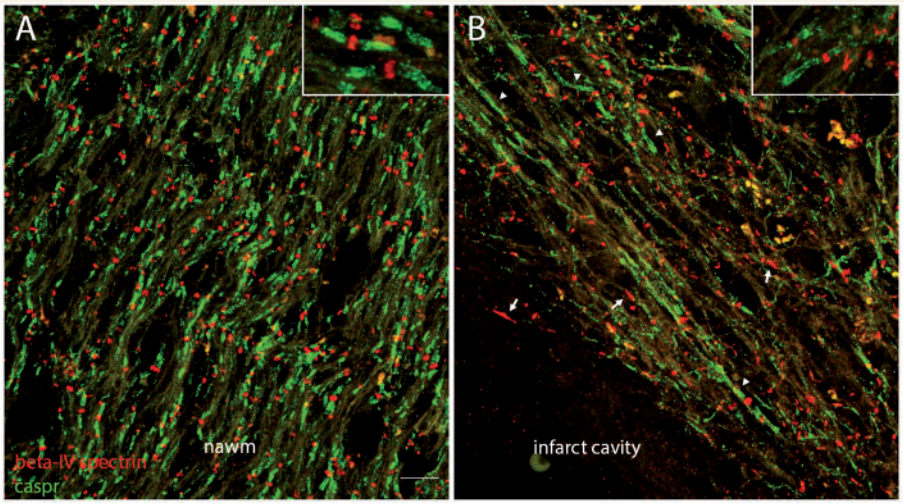

Figure 1 Nodal and paranodal abnormalities in axons adjacent to lacunar infarcts. Immunofluorescent labelling of nodal and paranodal regions in normal-appearing white matter (nawm) from an index case located away from regions of ischaemia (**A**) reveals a regular pattern of nodal (red) and paranodal (green) staining. Beta-IV spectrin-positive nodes and caspr-positive paranodes demonstrate relatively uniform staining pattern in controls (inset, **A**). Adjacent to an infarct (**B**), the frequency of intact nodal and paranodal staining is decreased. Elongated caspr-positive paranodal profiles (green) are apparent adjacent to the infarct (arrowheads and inset). Elongated beta-IV spectrin-positive nodal domains are also visible adjacent to the infarct (arrows). Magnification × 60. Scale bar = 10 μm.

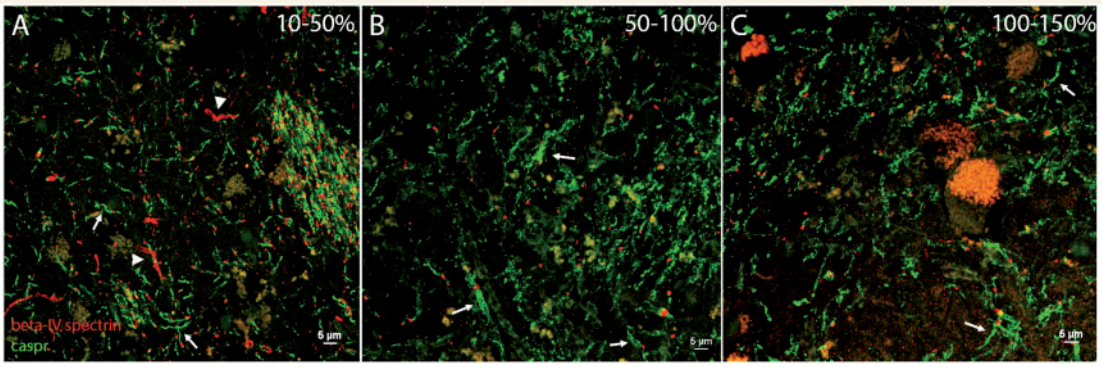

Figure 2 Abnormal nodal and paranodal profiles persist with increasing distance away from the infarct centre. Immediately adjacent to the infarct (10–50% of infarct diameter), elongated and irregular caspr-positive paranodes (green, arrows) are frequently seen (**A**). Beta-IV spectrin-positive nodal profiles (red) are also irregular (**A**). Further away from the infarct (50–100% of infarct diameter), axonal microdomains remain disrupted with irregular morphology of paranodal regions (arrows, **B**). In tissue adjacent to, but some distance from the infarct core (100–150% of infarct diameter), elongated paranodes (arrows) and irregular appearing nodal profiles persist (**C**). In some instances, beta-IV spectrin-positive axon initial segments are seen (arrowheads). Magnification × 60. Scale bar = 5 μm.

Molecular disorganization of specific proteins within the axon may reflect loss of myelin or other structural disruption of the axons. To examine the structural integrity of myelin and axons adjacent to lacunar infarcts, we labelled serial sections from each case for myelin basic protein (MBP) and neurofilament 200 (NF200) (Fig. 3). Although there is some evidence of denuded axons immediately adjacent to the infarct core (Fig. 3A), high magnification images at increasing distances from the infarct core reveal relative preservation of myelin and axons as evidenced by the close co-localization of MBP and NF200 staining (Fig. 3B–D). MBP and NF200 staining of age-matched control tissue shows a similar pattern of staining in both densely packed white matter (Supplementary Fig. 5C) and typical subcortical regions where lacunar strokes were located (Supplementary Fig. 5D). These data indicate that the molecular reorganization occurring at the node and paranode is not a result of lost myelin or structurally abnormal axons.

Molecular organization of axons in autosomal dominant RVCL

Autosomal dominant RVCL is a group of heritable stroke syndromes resulting from a mutation in the *TREX1* gene (Richards *et al.*, 2007; Kolar *et al.*, 2014) resulting in a

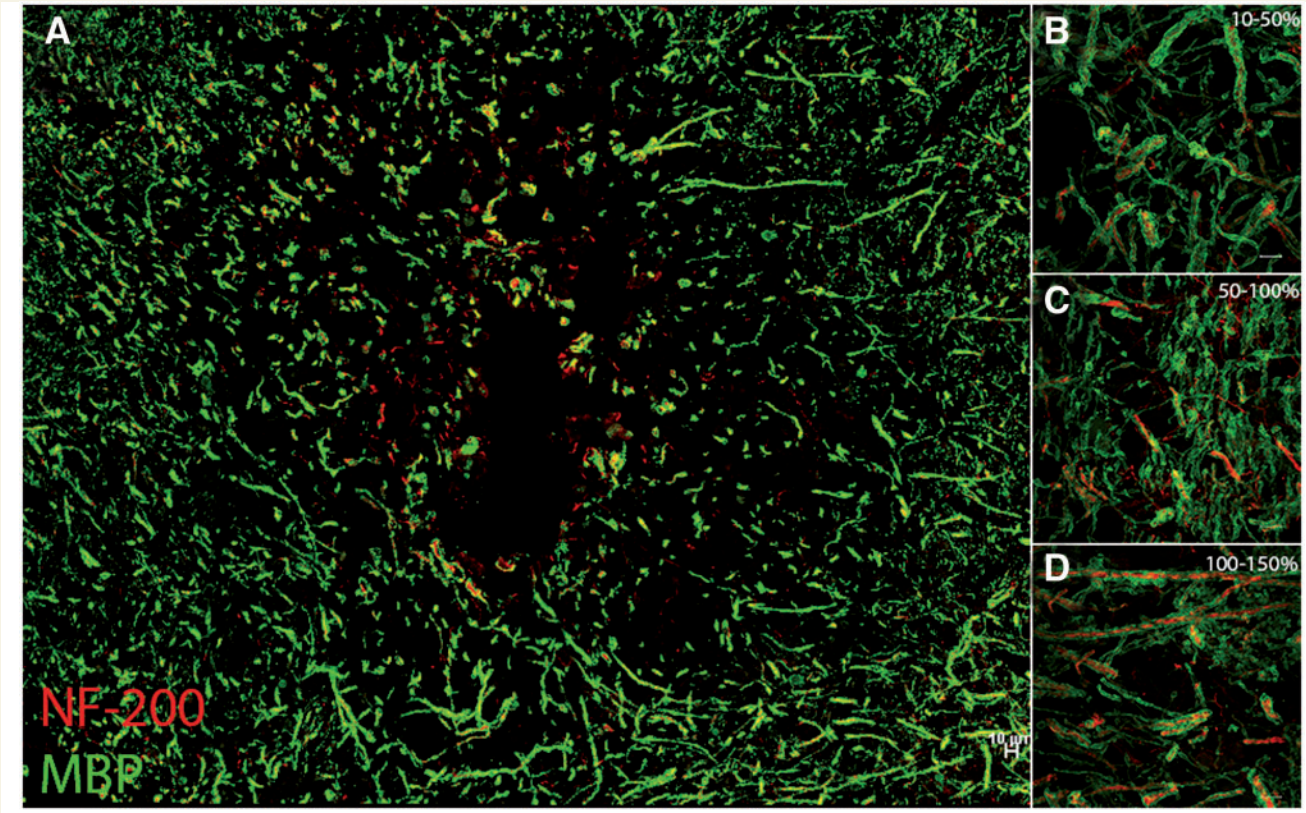

Figure 3 Molecular disorganization of axons adjacent to lacunar infarcts exists in the absence of significant changes in structural integrity of myelin and axons. Lacunar infarct stained for myelin basic protein (MBP, green) and neurofilament-200 (NF200, red) demonstrate some demyelinated axons immediately adjacent to infarct (**A**). Note that this image is a serial section of the infarct shown in Supplementary Fig. 1. Higher resolution confocal microscopic images of myelinated axons in increasing distance (**B**–**D**) from the infarct show that the structural integrity of axons and myelin remains largely intact despite significant changes in nodal and paranodal length as evidenced by beta-IV spectrin and caspr staining. Tiled confocal image at × 60 (**A**) and × 100 magnification (**B**–**D**). Scale bars = 10 μm.

multilayered capillary basement membrane (Jen *et al.*, 1997) that is thought to contribute to delayed and progressive infarction within the brain. These patients develop multiple small vessel infarcts within the cerebral white matter that accumulate over time and produce progressive neuropsychiatric decline. We hypothesized that such patients with repeated microvascular infarcts and multiple lacunar strokes would have similar molecular disorganization of axons adjacent to infarcts as we observed in routine clinical cases. In addition, these cases lack the potential confound of other forms of dementia such as Alzheimer's disease or frontotemporal dementia. They also demonstrate disease much earlier in life (Table 1) thus demonstrating that our results are not simply age-related. These cases also had clinical MRI images that would allow us to specifically examine brain areas that corresponded to regions of lacunar infarction and white matter hyperintensity.

Representative axial FLAIR and T_2-weighted images from one RVCL patient, demonstrate cystic, partially cavitated lacunar infarcts with adjacent white matter hyperintensity (Fig. 4A and B). Serial imaging available in these patients indicated progressive white matter damage, ultimately resulting in cystic lacunar infarcts (data not shown). Using this neuroimaging as a guide, we selected post-mortem brain blocks that included areas of T_2/FLAIR hyperintensity such as the right periventricular white matter for a detailed examination of axonal microdomain regions within the white matter of these patients.

Histological analysis of periventricular white matter from patients with RVCL demonstrates irregularly thickened capillary walls, thought to be central to the pathophysiology of the syndrome (Fig. 5A). Cavitary lacunar infarction could be found adjacent to the head of the caudate nucleus in histological sections from the region depicted in the box in Fig. 5B (Supplementary Fig. 6) as well as in regions of right frontal leukoencephalopathy (data not shown). Axonal microdomain integrity in nodes and paranodes in increasing tertiles away from the infarct, demonstrated elongated paranodes mostly immediately adjacent to the infarct (Supplementary Fig. 7). The limited sample of lacunar infarcts in these two cases prevented a detailed quantitative analysis of nodal and paranodal length.

In addition to these lacunar infarcts, multiple small pale regions consistent with microinfarcts were present within the white matter of patients with RVCL (Fig. 5A). Many

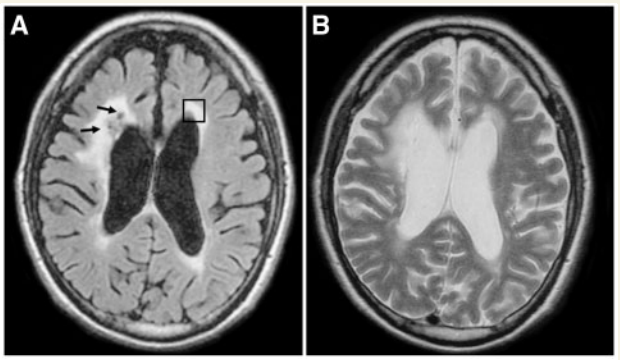

Figure 4 Representative axial FLAIR and T_2-weighted MRI images from one patient with autosomal dominant RVCL. FLAIR sequences demonstrate multiple periventricular lacunar infarcts, predominantly in the right frontal periventricular white matter (arrows, **A**) along with more diffuse FLAIR hyperintensity within the same regions. T_2-weighted images demonstrate both CSF-signal intensity lacunar infarcts as well as hyperintense signal change within the periatrial white matter (**B**). Immunofluorescently stained sections were taken from brain blocks corresponding to the left periventricular white matter (box) in **A**.

lesions also featured hyperpigmented microcalcinosis (Fig. 5B). In both cases, immunolabelling of nodal and paranodal regions within the white matter adjacent to these multiple microinfarcts reveals abnormal appearing paranodes (insets, Fig. 5C and D) and abnormal appearing nodal regions (Fig. 5C and D). In this limited sample, nodal length increased by 37.5% (1.21 μm) compared to control (0.88 μm) ($P < 0.0001$). Average paranodal length also increased by 8.75% (2.35 μm) compared to control (2.16 μm) ($P < 0.0001$). Overall, axonal microdomain analysis in the white matter of patients with RVCL demonstrates a consistent finding of disrupted axoglial cell-cell adhesion at paranodes in axons surviving white matter infarcts as we observed in non-heritable lacunar stroke.

Discussion

Cerebral microvascular disease leads to a spectrum of clinical syndromes that range from acute stroke to progressive cognitive decline and dementia. The disease is common and often unrecognized, making it vital to enhance our understanding of the disease process. Our findings demonstrate the relative preservation of myelin and the basic cytoskeletal structure of axons in regions adjacent to lacunar infarcts, while showing that the normal molecular organization of axons at nodes of Ranvier and flanking paranodal segments is disrupted. These results also demonstrate that similar findings are present in both classic type I cavitated lacunar lesions as well as microinfarcts, as we did not detect any difference in nodal or paranodal length between these different lesions. These findings generally support the concept of a region adjacent to existing white matter lesions that is susceptible to further injury as suggested by imaging studies (Maillard *et al.*, 2011; Duering *et al.*, 2013) and shows that this adjacent region may extend a significant distance from the central core lesion. The inclusion of surrounding axons in the spectrum of damage after white matter infarcts may explain the progressive nature of these lesions (Gouw *et al.*, 2008) as molecularly unstable axons degenerate over time. The presence of a white matter penumbral injury with surviving but damaged axons may also explain why clinical disability persists even after small strokes (Smith *et al.*, 2005, 2011; Nedeltchev *et al.*, 2007; Coutts *et al.*, 2012).

We observed a similar disruption of the molecular organization of axons in the white matter of two cases of autosomal dominant RVCL, demonstrating similar effects of cerebral microvascular disease on white matter and axons. By demonstrating similar findings in patients with RVCL who were substantially younger in age and lacking any pre-morbid confounding diagnosis of dementia when compared to our larger case series, we have shown that the molecular disorganization of axons adjacent to white matter stroke occurs independently of these variables. This finding suggests that an important consequence of cerebral microvascular disease is disruption of the normal axoglial relationship at paranodes. In addition, the targeted use of pre-morbid MRI studies in two cases of autosomal dominant RVCL to select post-mortem brain blocks for detailed tissue analysis provides an imaging-to-molecular neuropathology correlation that has not been previously reported. Using this approach, the pathological correlates of white matter hyperintensities can be better substantiated and provide new insights into the significance of white matter lesions on imaging.

Much of our understanding about the normal molecular organization of axons has been gleaned from mouse models (Susuki and Rasband, 2008). Node of Ranvier formation occurs through an orchestrated combination of extracellular matrix proteoglycans that trap neurofascin-186 at the node, axoglial junctions that develop at paranodes, and axonal cytoskeletal scaffolds that anchor key functional proteins such as Na_V (Susuki *et al.*, 2013). The tripartite molecular complex present at paranodes, including neurofascin-155, contactin, and contactin-associated protein (caspr, now known as CNTNAP1), is required to maintain the normal distribution of axonal ionic channels and functional saltatory conduction (Bhat *et al.*, 2001; Boyle *et al.*, 2001; Pillai *et al.*, 2009). In multiple sclerosis and its animal model, experimental autoimmune encephalomyelitis (EAE), autoimmune attack on myelin results in a loss of axoglial contact at paranodes and dispersion of nodal Na_V along the axon (Howell *et al.*, 2006; Herrero-Herranz *et al.*, 2008). Redistribution of Na_V outside of the nodal region is hypothesized to contribute to progressive axonal loss (Wingerchuk *et al.*, 2001). In a mouse model of cerebral hypoperfusion established by mild bilateral carotid narrowing, axoglial contact is also jeopardized with resultant increase in nodal and paranodal length (Reimer *et al.*,

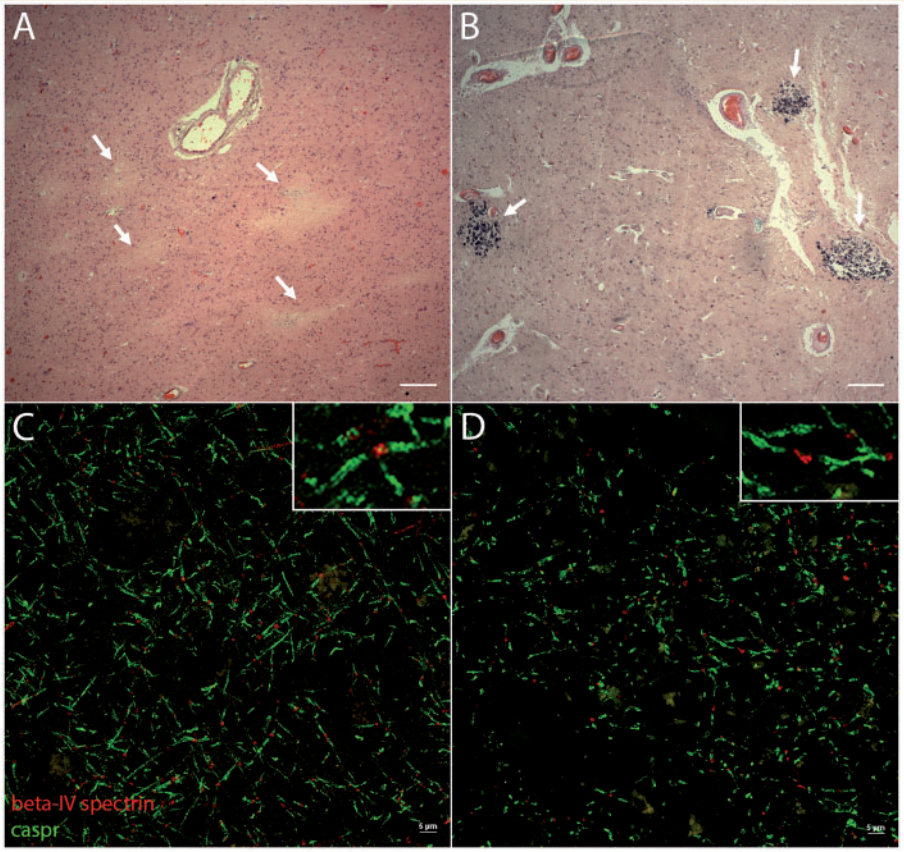

Figure 5 Microinfarcts and molecular disorganization of axons within the white matter of two patients with autosomal dominant retinal vasculopathy and cerebral leukoencephalopathy. Haematoxylin-eosin stained sections from periventricular white matter from two patients with autosomal dominant RVCL. (**A** and **B**) Multiple microinfarcts are present throughout the white matter (arrows). In Case 2, many of these microinfarcts were associated with the deposition of calcium within the lesions (arrows, **B**). In Case 1, most nodal segments (red) appear largely intact while paranodal segment (green) elongation is obvious throughout the white matter adjacent to microinfarcts (**C**, inset). In Case 2, a greater degree of axonal disruption is present adjacent to microinfarcts (**D**). Nodal abnormalities were more frequent and paranodal segments were also notably elongated (inset). Magnification $\times 60$. Scale bar = 5 μm.

2011). Thus, the phenomena of increased nodal and paranodal length serves as a common molecular marker of disrupted axoglial contact and signalling and signals impending damage to axons that are otherwise structurally intact.

Our findings suggest that the hyperintense signal change seen on MRI in ischaemic white matter includes regions of axons that lack the normal molecular organization needed for long-term survival and high-fidelity neurotransmission. Such a conclusion supports the data from human imaging studies showing that fractional anisotropy is decreased adjacent to existing regions of white matter hyperintensity (Maillard *et al.*, 2011). In fact, increases in mean diffusivity on MRI have been reported in normal-appearing white matter both in aged subjects (Bastin *et al.*, 2009) and in post-mortem *ex vivo* samples of spinal cord from patients with multiple sclerosis (Zollinger *et al.*, 2011). Chronic cerebral hypoperfusion in mice results in decreased fractional anisotropy and magnetic transfer ratios within the white matter (Holland *et al.*, 2011) and produces an increase in nodal and paranodal length (Reimer *et al.*, 2011). Although in the present study we focused on axonal molecular abnormalities adjacent to measurable lacunar infarcts, our findings may be applicable to imaging evidence of changes in more subtle white matter hyperintensities and normal-appearing white matter as well. Importantly, age-related increases in paranodal length are known to occur in rhesus monkeys and rats (Hinman *et al.*, 2006), thus any determination of axonal microdomain integrity in normal-appearing white matter must be considered in the context of normal age-related changes as we did here by using both internal and external controls.

White matter adjacent to an ischaemic lesion likely experiences partial injury to both oligodendrocytes and axons that is not sufficient to lead to cell death or trigger Wallerian degeneration, but nonetheless disrupts axoglial adhesion and trophic signalling through unknown mechanisms. This could be triggered by a gradient of ischaemia extending away from the central core of infarction supporting the traditional penumbral concept. Alternatively these changes may result from downstream paracrine inflammatory or other molecular signals initiated by the primary

ischaemic insult or by a decrease in blood–brain barrier integrity within the white matter (Wardlaw *et al.*, 2008) that would alter ionic gradients and bring systemic inflammatory cells to the area. Regardless of the trigger, the inability to transition back to a stable axoglial relationship results in progressive axonal degeneration in the region adjacent to the initial injury. Such a concept is supported again by serial human imaging studies identifying that new lesions appear adjacent to prior areas of injury (Gouw *et al.*, 2008; Duering *et al.*, 2013) as well as by transgenic mice lacking the key paranodal protein NF155 that undergo a progressive axonal degeneration in the absence of stable axoglial junctions (Pillai *et al.*, 2009). Thus, an enhanced understanding of the molecular systems that maintain axoglial contact and the effect of stroke on these systems is needed.

In conclusion, we have demonstrated that traditional imaging and histopathological methods underestimate the degree of damage resulting from white matter injury. Histology has previously been shown to be superior to post-mortem MRI in demonstrating the extent of damage within white matter (Fernando *et al.*, 2004). Here, we show that a molecular neuropathological approach is capable of demonstrating that the molecular disorganization of axons exists a substantial distance from the infarct core, further supporting the concept of a white matter penumbra. Within this penumbra are surviving but damaged axons, marked by axonal microdomain disorganization, that fail to maintain contact with oligodendrocytes and lose the molecular underpinnings of saltatory conduction. These surviving but impaired axons can contribute to progressive axonal loss and disability. In addition, we also show that the combined use of neuroimaging and molecular pathology can help to identify the spectrum of injuries that underlie white matter hyperintensity on MRI. Future studies should use a similar approach and sample the brain more widely to determine the degree to which these changes are relevant to the white matter as a whole. In turn, this knowledge can identify new therapeutic targets to protect white matter from progressive injury and promote neural repair.

Acknowledgements

We thank Joanna Jen for the identification and sharing of clinical cases, insightful discussions, and review of the manuscript.

Funding

This work was gratefully supported by the NIH. J.D.H. was supported by NINDS: K08NS083740 and R25NS065723. S.T.C. received support from NS071481. H.V.V. and S.T. were supported in part by NIA: P50AG16570, P01AG12435, and the UCLA Mary Easton Alzheimer's Disease Research Centre.

Supplementary material

Supplementary material is available at *Brain* online.

References

Arsava EM, Bayrlee A, VAngel M, Rost NS, Rosand J, Furie KL, et al. Severity of leukoaraiosis determines clinical phenotype after brain infarction. Neurology 2011; 77: 55–61.

Bailey EL, Smith C, Sudlow CL, Wardlaw JM. Pathology of lacunar ischaemic stroke in humans—a systematic review. Brain Pathol 2012; 22: 583–91.

Bastin ME, Clayden JD, Pattie A, Gerrish IF, Wardlaw JM, Deary IJ. Diffusion tensor and magnetization transfer MRI measurements of periventricular white matter hyperintensities in old age. Neurobiol Aging 2009; 30: 125–36.

Bhat MA, Rios JC, Lu Y, Garcia-Fresco GP, Ching W, St Martin M, et al. Axon-glia interactions and the domain organization of myelinated axons requires neurexin IV/Caspr/Paranodin. Neuron 2001; 30: 369–83.

Boyle ME, Berglund EO, Murai KK, Weber L, Peles E, Ranscht B. Contactin orchestrates assembly of the septate-like junctions at the paranode in myelinated peripheral nerve. Neuron 2001; 30: 385–97.

Brundel M, de Bresser J, van Dillen JJ, Kappelle LJ, Biessels GJ. Cerebral microinfarcts: a systematic review of neuropathological studies. J Cereb Blood Flow Metab 2012; 32: 425–36.

Conijn MM, Kloppenborg RP, Algra A, Mali WP, Kappelle LJ, Vincken KL, et al. Cerebral small vessel disease and risk of death, ischaemic stroke, and cardiac complications in patients with atherosclerotic disease: the Second Manifestations of ARTerial disease-Magnetic Resonance (SMART-MR) study. Stroke 2011; 42: 3105–9.

Coutts SB, Modi J, Patel SK, Aram H, Demchuk AM, Goyal M, Hill MD. What causes disability after transient ischaemic attack and minor stroke?: results from the CT and MRI in the triage of TIA and minor Cerebrovascular events to identify high risk patients (CATCH) study. Stroke 2012; 43: 3018–22.

Decarli C. Clinically asymptomatic vascular brain injury: a potent cause of cognitive impairment among older individuals. J Alzheimer's Dis 2013; 33 (Suppl 1): S417–26.

Duering M, Csanadi E, Gesierich B, Jouvent E, Herve D, Seiler S, et al. Incident lacunes preferentially localize to the edge of white matter hyperintensities: insights into the pathophysiology of cerebral small vessel disease. Brain 2013; 136: 2717–26.

Dupree JL, Girault JA, Popko B. Axo-glial interactions regulate the localization of axonal paranodal proteins. J Cell Biol 1999; 147: 1145–52.

Einheber S, Zanazzi G, Ching W, Scherer S, Milner TA, Peles E, et al. The axonal membrane protein Caspr, a homologue of neurexin IV, is a component of the septate-like paranodal junctions that assemble during myelination. J Cell Biol 1997; 139: 1495–506.

Fernando MS, O'brien JT, Perry RH, English P, Forster G, Mcmeekin W, et al. Comparison of the pathology of cerebral white matter with post-mortem magnetic resonance imaging (MRI) in the elderly brain. Neuropathol Appl Neurobiol 2004; 30: 385–95.

Ferrer I, Kaste M, Kalimo H. Consequences of cerebrovascular disorders. In: Love S, Louis D, Ellison DW, editors. Greenfield's neuropathology. 8th edn. Boca Raton, FL: CRC Press; 2008.

Fisher CM. Lacunar strokes and infarcts: a review. Neurology 1982; 32: 871–6.

Go AS, Mozaffarian D, Roger VL, Benjamin EJ, Berry JD, Blaha MJ, et al. Heart disease and stroke statistics—2014 update: a report from the American heart association. Circulation 2014; 129: e28–e292.

Gouw AA, Van der Flier WM, Fazekas F, van Straaten EC, Pantoni L, Poggesi A, et al. Progression of white matter hyperintensities and

incidence of new lacunes over a 3-year period: the Leukoaraiosis and Disability study. Stroke 2008; 39: 1414–20.

Herrero-Herranz E, Pardo LA, Gold R, Linker RA. Pattern of axonal injury in murine myelin oligodendrocyte glycoprotein induced experimental autoimmune encephalomyelitis: implications for multiple sclerosis. Neurobiol Dis 2008; 30: 162–73.

Hinman JD, Peters A, Cabral H, Rosene DL, Hollander W, Rasband MN, et al. Age-related molecular reorganization at the node of Ranvier. J Comp Neurol 2006; 495: 351–62.

Holland PR, Bastin ME, Jansen MA, Merrifield GD, Coltman RB, Scott F, et al. MRI is a sensitive marker of subtle white matter pathology in hypoperfused mice. Neurobiol Aging 2011; 32: 2325 e1–6.

Howell OW, Palser A, Polito A, Melrose S, Zonta B, Scheiermann C, et al. Disruption of neurofascin localization reveals early changes preceding demyelination and remyelination in multiple sclerosis. Brain 2006; 129: 3173–85.

Jen J, Cohen AH, Yue Q, Stout JT, Vinters HV, Nelson S, et al. Hereditary endotheliopathy with retinopathy, nephropathy, and stroke (HERNS). Neurology 1997; 49: 1322–30.

Kolar GR, Kothari PH, Khanlou N, Jen JC, Schmidt RE, Vinters HV. Neuropathology and genetics of cerebroretinal vasculopathies. Brain Pathol 2014; 24: 510–8.

Maillard P, Fletcher E, Harvey D, Carmichael O, Reed B, Mungas D, et al. White matter hyperintensity penumbra. Stroke 2011; 42: 1917–22.

Nedeltchev K, Schwegler B, Haefeli T, Brekenfeld C, Gralla J, Fischer U, et al. Outcome of stroke with mild or rapidly improving symptoms. Stroke 2007; 38: 2531–5.

Okamoto Y, Ihara M, Fujita Y, Ito H, Takahashi R, Tomimoto H. Cortical microinfarcts in Alzheimer's disease and subcortical vascular dementia. Neuroreport 2009; 20: 990–6.

Pillai AM, Thaxton C, Pribisko AL, Cheng JG, Dupree JL, Bhat MA. Spatiotemporal ablation of myelinating glia-specific neurofascin (Nfasc NF155) in mice reveals gradual loss of paranodal axoglial junctions and concomitant disorganization of axonal domains. J Neurosci Res 2009; 87: 1773–93.

Reimer MM, Mcqueen J, Searcy L, Scullion G, Zonta B, Desmazieres A, et al. Rapid disruption of axon-glial integrity in response to mild cerebral hypoperfusion. J Neurosci 2011; 31: 18185–94.

Richards A, Van den Maagdenberg AM, Jen JC, Kavanagh D, Bertram P, Spitzer D, et al. C-terminal truncations in human 3'-5' DNA exonuclease TREX1 cause autosomal dominant retinal vasculopathy with cerebral leukodystrophy. Nat Genet 2007; 39: 1068–70.

Rios JC, Melendez-Vasquez CV, Einheber S, Lustig M, Grumet M, Hemperly J, et al. Contactin-associated protein (Caspr) and contactin form a complex that is targeted to the paranodal junctions during myelination. J Neurosci 2000; 20: 8354–64.

Roger VL, Go AS, Lloyd-Jones DM, Benjamin EJ, Berry JD, Borden WB, et al. Heart disease and stroke statistics—2012 update: a report from the American heart association. Circulation 2012; 125: e2–e220.

Schafer DP, Rasband MN. Glial regulation of the axonal membrane at nodes of Ranvier. Curr Opin Neurobiol 2006; 16: 508–14.

Smith EE, Abdullah AR, Petkovska I, Rosenthal E, Koroshetz WJ, Schwamm LH. Poor outcomes in patients who do not receive intravenous tissue plasminogen activator because of mild or improving ischaemic stroke. Stroke 2005; 36: 2497–9.

Smith EE, Fonarow GC, Reeves MJ, Cox M, Olson DM, Hernandez AF, et al. Outcomes in mild or rapidly improving stroke not treated with intravenous recombinant tissue-type plasminogen activator: findings from Get With The Guidelines-Stroke. Stroke 2011; 42: 3110–5.

Sonohara K, Kozaki K, Akishita M, Nagai K, Hasegawa H, Kuzuya M, et al. White matter lesions as a feature of cognitive impairment, low vitality and other symptoms of geriatric syndrome in the elderly. Geriatr Gerontol Int 2008; 8: 93–100.

Susuki K, Chang KJ, Zollinger DR, Liu Y, Ogawa Y, Eshed-Eisenbach Y, et al. Three mechanisms assemble central nervous system nodes of Ranvier. Neuron 2013; 78: 469–82.

Susuki K, Rasband MN. Molecular mechanisms of node of Ranvier formation. Curr Opin Cell Biol 2008; 20: 616–23.

Tait S, Gunn-Moore F, Collinson JM, Huang J, Lubetzki C, Pedraza L, et al. An oligodendrocyte cell adhesion molecule at the site of assembly of the paranodal axo-glial junction. J Cell Biol 2000; 150: 657–66.

van Veluw SJ, Zwanenburg JJ, Engelen-Lee J, Spliet WG, Hendrikse J, Luijten PR, et al. *In vivo* detection of cerebral cortical microinfarcts with high-resolution 7T MRI. J Cereb Blood Flow Metab 2013; 33: 322–9.

Vermeer SE, Hollander M, van Dijk EJ, Hofman A, Koudstaal PJ, Breteler MM. Silent brain infarcts and white matter lesions increase stroke risk in the general population: the Rotterdam scan study. Stroke 2003; 34: 1126–9.

Vermeer SE, Longstreth WT, Jr, Koudstaal PJ. Silent brain infarcts: a systematic review. Lancet Neurol 2007; 6: 611–9.

Wardlaw JM, Farrall A, Armitage PA, Carpenter T, Chappell F, Doubal F, et al. Changes in background blood-brain barrier integrity between lacunar and cortical ischaemic stroke subtypes. Stroke 2008; 39: 1327–32.

Wingerchuk DM, Lucchinetti CF, Noseworthy JH. Multiple sclerosis: current pathophysiological concepts. Lab Invest 2001; 81: 263–81.

Zollinger LV, Kim TH, Hill K, Jeong EK, Rose JW. Using diffusion tensor imaging and immunofluorescent assay to evaluate the pathology of multiple sclerosis. J Magn Reson Imaging 2011; 33: 557–64.